

Local Organization of Biological Membranes Modulates Tau–Lipid Interactions and Fibril formation

Clara Piersson, Victoria Lublin, Mathieu Duttine, Lucie Khemtemourian, Antoine Loquet, Marion Mathelié-Guinlet, and Yann Fichou*



Cite This: <https://doi.org/10.1021/jacsau.6c00374>



Read Online

ACCESS |



Metrics & More



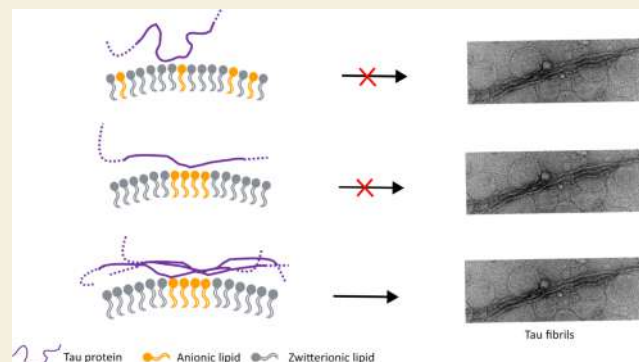
Article Recommendations



Supporting Information

ABSTRACT: The formation of Tau amyloids is a hallmark of several neurodegenerative diseases, called Tauopathies, including Alzheimer's disease. In different Tauopathies, Tau amyloid filaments adopt a distinct structure, highlighting the existence of disease specific pathways. In this pathological context, lipid metabolism is heavily disrupted, leading to a perturbation of membrane composition. Lipid membranes have been shown to nucleate tau aggregation under some conditions. However, no general model has been established to explain how the organization of the lipid membrane modulates Tau aggregation. Here, we combined biochemistry and biophysical tools, including EPR spectroscopy, to investigate the mechanisms of membrane-induced Tau aggregation. After showing the importance of the electrostatic interaction between Tau and anionic lipids, we investigate how the amount and density of charges influence Tau aggregation. This work allows us to draw a general model where membrane-induced Tau aggregation is a two-step process. First, the binding to the membrane through electrostatic interactions is a necessary but not a sufficient step. Second, the nucleation of Tau amyloids at the membrane surface occurs only when specific conditions are fulfilled, i.e., high surface density altering Tau conformation and spatial proximity between aggregation-prone conformers. A direct implication of this model is that local membrane heterogeneities, such as phase separation or lipid rafting, are strong modulators of Tau aggregation. This work provides the molecular basis to predict how different membrane states regulate Tau aggregation.

KEYWORDS: Tau protein, lipid membrane, amyloid, aggregation mechanism, EPR spectroscopy



1. INTRODUCTION

Tau is an intrinsically disordered protein predominantly expressed in neurons, where it plays a key physiological role in stabilizing microtubules. Tau exists as six isoforms ranging from 352 to 441 amino acids. These isoforms are defined by the presence of two N-terminal inserts (N1 and N2) and by the inclusion of the second repeat domain (R2) within the C-terminal domain. The longest isoform, containing both N-terminal inserts and all four repeat domains, is referred to as 2N4R. Pathologically, insoluble Tau aggregates are a hallmark of several neurodegenerative disorders, collectively known as Tauopathies,¹ including Alzheimer's disease. These aggregates are formed of amyloid fibrils characterized by a cross- β structure, in which highly ordered β -sheets stack along the fibril axis.² Several pathogenic mutations of Tau have been identified in tauopathies, among which the P301L mutation in the MAPT gene is particularly well characterized and widely used as a model because it robustly enhances Tau amyloid aggregation.³ In recent years, high-resolution structures of Tau fibrils from different Tauopathies have been resolved, revealing the presence of nonproteinaceous densities both within and surrounding the

fibril core.^{4–8} These additional densities are thought to correspond to either post-translational modifications or tightly bound cofactors. In parallel, lipid components such as phosphatidylcholine, cholesterol, and sphingolipids have been found to colocalize with Tau fibrils in Alzheimer's disease brain tissue, suggesting a direct association between lipids and pathological Tau assemblies.⁹ Besides, lipid metabolism has been shown to be altered in pathological contexts, with elevated levels of phospholipids and sphingolipids detected in the transgenic rat brain, cerebrospinal fluid, and plasma.¹⁰ Although it remains unclear whether these lipids contribute to the observed nonproteinaceous densities, their presence raises the possibility that lipids could be among the molecular partners embedded within the fibrils, as recently observed for α -synuclein⁵⁹

Received: March 12, 2026

Revised: April 9, 2026

Accepted: April 10, 2026

lipidic fibrils.¹¹ Supporting this, Tau has been shown to interact with the plasma membrane¹² and to translocate across it via both direct membrane crossing and vesicle-mediated pathways, facilitating its intercellular propagation.^{13–15} Particularly, lipid rafts have also been implicated in the spatial localization and accumulation of neurodegeneration-associated molecules, including phosphorylated Tau.¹⁶

The study of Tau's interaction with and aggregation on model membranes is an area of growing interest. Tau's interaction with lipids has mostly focused on the repeat region,¹⁷ which engages in electrostatic interactions with negatively charged lipids such as phosphatidylserine (PS)¹⁸ and phosphatidylinositol-4,5-bisphosphate (PIP2),¹⁹ although the N-terminal region was suggested to have an important role in Tau–membrane interaction.²⁰ Yet, how the composition and organization of membranes modulate their interaction with Tau and their capacity to induce Tau amyloid aggregation has been scarcely studied. In particular, there are no general models allowing one to predict how disease-relevant membrane alteration, such as lipid composition modification, can influence Tau aggregation. In this study, we investigated the interaction and aggregation of the full-length Tau protein in the presence of lipid membranes composed of varying anionic/zwitterionic lipid ratios, using electron paramagnetic resonance (EPR) spectroscopy, fluorescence assays, and transmission electron microscopy (TEM) to monitor membrane binding and fibril formation. We examined how Tau binds to membranes and highlight the local membrane anionic charge density as a key parameter in promoting a two-step aggregation mechanism. In particular, we show that the initial protein–membrane interaction is mostly dependent on electrostatic interaction, while the subsequent amyloid nucleation depends on a conformational change around the PHF6 motif that is highly dependent on the membrane organization.

2. METHODS

2.1. Production and Purification of Tau

The longest isoform of Tau (2N4R) containing the disease-associated mutation P301L was expressed in *Escherichia coli* BL21(DE3) cells transformed with a pET28 plasmid encoding the corresponding gene.

A 10 mL overnight preculture was used to inoculate 1 L of the LB medium supplemented with kanamycin (30 μ g/mL). Cultures were incubated at 37 °C with shaking at 200 rpm until an optical density at 600 nm (OD₆₀₀) of 0.6–0.8 was reached. Protein expression was induced with 1 mM IPTG, followed by a 3 h incubation at 37 °C and 200 rpm. Cells were harvested by centrifugation at 5000 rpm for 20 min at 4 °C. The resulting pellet was resuspended in 30 mL of lysis buffer (50 mM Tris-HCl, pH 7.4, 100 mM NaCl, 0.1 mM EDTA) supplemented with 1 mM PMSF, 5 mM DTT, 20 μ g/mL DNase I, 10 mM MgCl₂, and one protease inhibitor tablet. Cells were lysed by the addition of lysozyme (70 mg/mL) and incubation at room temperature for 30 min with agitation, followed by three cycles of freeze–thaw in liquid nitrogen. Cell debris were removed by centrifugation at 9500 rpm for 10 min at 4 °C. The supernatant was subjected to a heat denaturation step at 75 °C for 12 min, followed by cooling on ice for 20 min. PMSF was added prior to a second centrifugation at 9500 rpm for 10 min at 4 °C to remove precipitated proteins. The resulting supernatant was filtered and subsequently loaded onto a Bio-Rad NGC FPLC system for purification.

The first purification step was cation exchange chromatography. The Tau-containing lysate was loaded onto a 5 mL EconoFit UNO Sphere S column (Bio-Rad) pre-equilibrated with 20 mM sodium phosphate buffer at pH 7.4, 0.1 mM EDTA, and 100 mM NaCl. The column was washed with seven column volumes (CV) of equilibration buffer prior to elution. Elution was performed using a linear gradient of NaCl (up to

500 mM), from 0 to 60% over one CV, followed by a step to 100% over three CVs. Fractions corresponding to the eluted protein peak were pooled and concentrated to a final volume of 5 mL. The sample was then applied to size-exclusion chromatography using a Superdex 200 Increase 16/600 pg column (Cytiva), pre-equilibrated with 20 mM HEPES at pH 7.4 and 100 mM NaCl. Eluted fractions containing pure Tau protein were pooled, concentrated, and quantified by UV absorbance at 274 nm using an extinction coefficient of 7.5 mM^{−1}·cm^{−1}. The final purified protein was stored at −20 °C.

2.2. Liposome Formulation into Large Unilamellar Vesicles (LUVs)

Large unilamellar vesicles (LUVs) composed of physiologically relevant phospholipids, such as 1-palmitoyl-2-oleoyl-*sn*-glycero-3-phospho-L-serine (POPS), 1-palmitoyl-2-oleoyl-glycero-3-phosphocholine (POPC), 1,2-distearoyl-*sn*-glycero-3-phosphocholine (DSPC), or phosphatidylinositol-4,5-bisphosphate (PIP2), were prepared. The lipids, initially dissolved in chloroform, were mixed at a defined molar ratio and dried under a nitrogen stream to form a lipid film. This film was then placed under a vacuum in a desiccator overnight to remove residual traces of chloroform.

The lipid film was subsequently solubilized in a 20 mM HEPES buffer at pH 7.4. The lipid suspension then underwent five freeze–thaw cycles using liquid nitrogen. To ensure that both lipids were in the fluid phase, the solution was maintained at 40 °C (or 55 °C when using DSPC). Finally, the suspension was extruded 21 times through membranes with 100 nm pores to obtain LUVs. The vesicle size was assessed by dynamic light scattering (DLS, Cordouan), and the lipid concentration was determined by the phosphate assay, following a previously described method.²¹

2.3. Thioflavin T Aggregation

Thioflavin T (ThT) is a fluorescent dye that specifically binds to β -sheet structures of amyloid proteins.²² ThT assays were conducted in a 384-well low-volume black microplate with a clear flat bottom; Tau protein was incubated at 20 μ M with or without lipids in 20 mM HEPES at pH 7.4 and 5 mM DTT and with 20 μ M ThT for 2 days at 37 °C with shaking at 300 rpm. The fluorescence was bottom read in a BMG Vantastar instrument with excitation and emission wavelengths of 440 and 480 nm, respectively. Each condition was prepared independently in three different wells. Standard deviation over these three wells is represented as error bars throughout the manuscript.

2.4. Transmission Electron Microscopy

The carbon film 300 mesh copper grids were hydrophilized by UV light for 5 min. Four μ L of samples were applied on the grid for 2 min before applying the staining solution. Four μ L of 2% uranyl acetate filtered was applied on the grid twice for 1 min. Samples were imaged with an FEI CM120 operated at 80 kV. Images were recorded with a USC1000 slow scan CCD camera (Gatan, Pleasanton, CA, USA).

2.5. Atomic Force Microscopy

Supported lipid bilayers (SLBs) were prepared for AFM experiments by depositing 100 μ L of 0.25 mg/mL POPS/POPC (50/50) and POPS/DSPC (20/80 and 50/50) SUV suspensions, along with 1 mM CaCl₂, onto freshly cleaved mica. The samples were incubated at room temperature for 30 min. Following incubation, the samples were rinsed five times with buffer (20 mM HEPES, pH 7.4, 100 mM NaCl).

AFM imaging was conducted using the Dimension FastScan system (Bruker), operating in PeakForce Quantitative NanoMechanics (PF-QNM) mode in a liquid environment at room temperature (~25 °C).

2.6. Spin Labeling for Electron Paramagnetic Resonance

Site-directed mutagenesis was applied to 2N4R-P301L in order to obtain three mutants containing a single cysteine for CW-EPR: C291S (cysteine present at position 322), C322S (cysteine present at position 291), and C291S–C322S–S46C (cysteine present at position 46). Similarly, the mutations C291S–C322S–V300C–V313C were added for DEER experiments.

Tau mutants were labeled on cysteine residues using the nitroxide spin-label MTSL (CAS 81213–52–7). Prior to labeling, Tau was reduced with TCEP for 2 h at room temperature. TCEP was then

184 removed using a PD-10 desalting column. A 10-fold molar excess of
 185 MTSL was subsequently added, and the mixture was incubated for a
 186 minimum of 2 h under continuous stirring. Excess spin labeling was
 187 eliminated by two successive PD-10 column purifications. The
 188 concentration of spin-labeled Tau was determined using a standard
 189 curve generated with TEMPO (10–500 μ M range), and signal
 190 integration (single and double integrals) was performed using
 191 SpinToolbox with a labeling efficiency ranging from 67 to 96%.

2.7. Continuous Wave-Electron Paramagnetic Resonance (CW-EPR)

193 Continuous wave-EPR (CW-EPR) measurements were carried out on a
 194 Bruker Elexsys E500 X-band spectrometer operating at 9.78 GHz. The
 195 microwave power was set to 6.3 mW, with a modulation amplitude of 1
 196 G and a sweep width of 100 G. Samples consisted of 20 μ L solutions
 197 containing 25 μ M Tau and various lipid compositions and ratios. Each
 198 sample was transferred to a 0.8 mm diameter quartz capillary for
 199 measurement at room temperature.

200 To determine the hyperfine coupling constants, additional measure-
 201 ments were performed under frozen conditions with a Bruker ESP300E
 202 X-band spectrometer operating at 9.54 GHz, equipped with a TE104
 203 rectangular resonator and an Oxford Instruments ESR900 helium-flow
 204 cryostat at 30 K using an optimized microwave power (2 mW) to avoid
 205 any saturation effect. For these experiments, samples containing 50 μ M
 206 spin-labeled Tau were prepared in the presence or absence of POPS at a
 207 Tau:lipid molar ratio of 1:125.

2.8. CW-EPR Spectra Fitting

208 Spectral simulations were conducted using SimLabel, a graphical
 209 interface built upon the EasySpin toolbox. All simulations were
 210 performed using the Chili routine with an isotropic rotation model.
 211 Experimental spectra corresponding to Tau in the monomeric state and
 212 in the presence of excess POPS (protein–lipid ratio of 1:250) were
 213 independently analyzed. In accordance with established protocols [2],
 214 distinct data sets were prepared for each experimental condition. The A_z
 215 component of the hyperfine interaction was first extracted from spectra
 216 acquired under frozen conditions, and the g_x value was subsequently
 217 calculated according to $g_x = f(A_z) = -0.0025 \times A_z + 2.0175$.²³ During
 218 the fitting process, the g_y and g_z components of the g-tensor were held
 219 constant. Fitted parameters were then the isotropic rotational
 220 correlation time (τ_{corr}), the axial hyperfine coupling constants ($A_x =$
 221 A_y), and a phenomenological Lorentzian broadening parameter. The
 222 latter was necessary to obtain an optimal fit of the monomeric state. A
 223 summary of the optimized parameters for all conditions is provided in
 224 Table 1.

Table 1. Fitting Parameters Obtained with Simlabel for the Tau Monomer and Tau Saturated with POPS, at Position 322

fitting parameters	Tau monomer	Tau saturated
g_x	2.0083	2.0087
g_y	2.0061	2.0061
g_z	2.0022	2.0022
$A_x = A_y$ (mT)	0.60	0.60
A_z (mT)	3.68	3.54
correlation time (ns)	0.375	2.52
Lorentzian width (MHz)	0.12	0

225 The percentage of bound protein was obtained for any spectra by
 226 fitting with a linear combination of the “monomer” and “saturated”
 227 component (Table 1) with SimLabel.

2.9. Binding Model Fitting

228 Binding curves were analyzed using a Hill model to quantify Tau–
 229 membrane interactions:

$$P + n_{\text{H}}L \rightleftharpoons P(L)_{n_{\text{H}}}$$

n_{H} is the Hill coefficient; it reflects the apparent degree of
 cooperativity when Tau (P) binds to the membrane (L). The apparent
 dissociation constant can be expressed as

$$K_{\text{D}} = \frac{[P][L]^{n_{\text{H}}}}{[P(L)_{n_{\text{H}}}]}$$

The fraction of Tau bound to the membrane is then defined as

$$\theta = \frac{[L]^{n_{\text{H}}}}{K_{50}^{n_{\text{H}}} + [L]^{n_{\text{H}}}}$$

where K_{50} is defined as the lipid concentration at half-maximal protein
 binding (i.e., $\theta = 0.5$). K_{50} represents an apparent dissociation constant,
 while n_{H} quantifies the apparent cooperativity of the interaction.

To compare multiple membrane compositions simultaneously, we
 performed a global nonlinear least-squares fit in which a single global
 K_{50} was shared across all data sets, while each lipid composition was
 allowed to have its own Hill coefficient n_{H} . The parameters were
 optimized using SciPy's least_squares, with bounds ensuring physically
 meaningful values ($K_{50} > 0$, $n_{\text{H}} > 0$). Standard errors were derived from
 the Jacobian-based covariance matrix.

2.10. Double Electron Electron Resonance (DEER)

DEER measurements were performed at Q-band on a Bruker E580
 pulsed EPR spectrometer equipped with a QD2 resonator (EN
 5107D2) and a 10 W solid-state microwave power amplifier at 60 K. To
 assess intramolecular distances while minimizing intermolecular
 contributions, doubly spin-labeled Tau (15 μ M) was mixed with a 4-
 fold excess of cysteine-free Tau (60 μ M) prior to freezing, in the
 presence or absence of LUVs of varying compositions and ratios. The
 final buffer contained 20 mM HEPES at pH 7.4 and 30% (v/v) glycerol,
 in a total volume of 20 μ L. Samples were incubated for 5–10 min and
 then flash-frozen in liquid nitrogen. Background correction was adapted
 to the geometry of the spin-label distribution, using a 3D model for Tau
 in solution and a 2D model when membrane-bound.

DEER measurements were performed using the standard four-pulse
 sequence: $\pi_{\text{obs}}/2 - \tau_1 - \pi_{\text{obs}} - (t - \pi_{\text{pump}}) - (\tau_2 - t) - \pi_{\text{obs}} - \tau_2 -$
 echo. Rectangular observer pulses were used with pulse lengths of 20
 ($\pi_{\text{obs}}/2$) and 40 ns (π_{obs}). Each DEER experiment was
 accumulated for approximately 12–24 h. Data were analyzed using
 the LongDistance software (<http://www.chemistry.ucla.edu/directory/hubbell-wayne-l>).

The background was obtained by fitting at long dipolar evolution
 time the function:

$$V(t) = V_0 \times e^{-\alpha t^{D/3}} \quad (1)$$

D was fixed to 2 for conditions where the protein interacts with a
 membrane. This dimensionality of 2 was verified to be accurate by
 measuring DEER of singly labeled Tau in interaction with membranes
 (Figure S1). D was set to 3 when Tau was in solution (no incubation
 with LUV). α and V_0 were fitted to the experimental traces. α is directly
 related to the local spin concentration.^{24,25}

3. RESULTS

In this study, we used full-length Tau (2N4R) with the
 aggregation-promoting disease mutation P301L (Figure 1A),
 hereafter referred to as Tau P301L. Large unilamellar vesicles
 (LUVs) composed of different lipids were extruded at about 150
 nm (Figure S2) to model biological membranes. We mostly used
 1-palmitoyl-2-oleoyl-sn-glycero-3-phospho-L-serine (POPS)
 and 1-palmitoyl-2-oleoyl-glycero-3-phosphocholine (POPC)
 to represent anionic and zwitterionic lipids, respectively. The
 lipid compositions of all membranes investigated in this work are
 listed in Table S1.

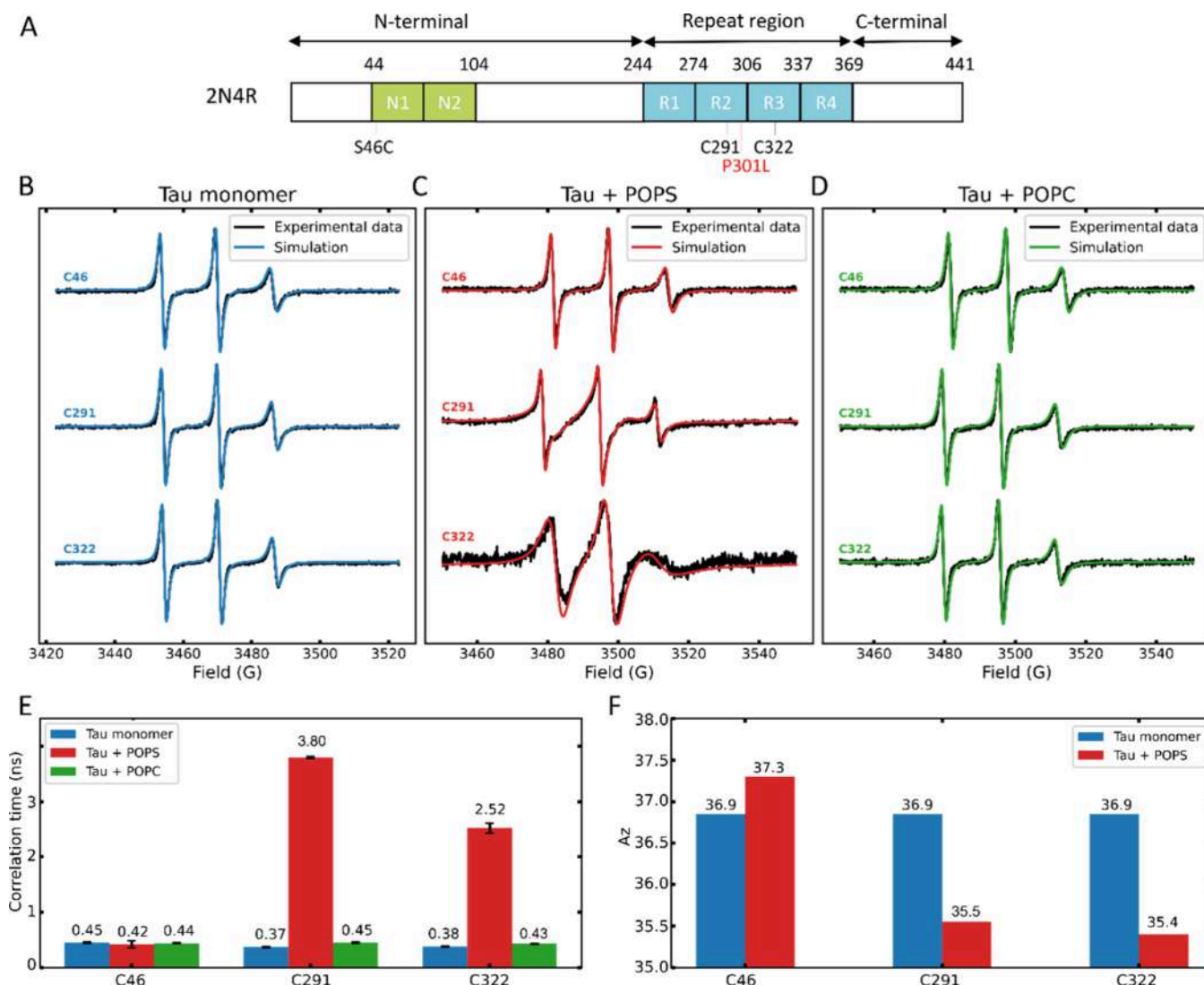


Figure 1. (A) Tau 2N4R sequence with P301L mutation and natural cysteines. CW-EPR characterizes the interaction of Tau with the membrane at residue sites 46, 291, and 322. Continuouswave-EPR spectra of Tau P301L in the (B) absence and (C) presence of POPS vesicles and (D) POPC vesicles (Tau/lipid molar ratio = 1:250, [Tau] = 25 μ M). Colored lines depict the simulation, which allows to extract a correlation time. (E) Correlation time for each site at the Tau/lipid ratio of 1:250. (F) Hyperfine constant A_z , which reflects the local polarity, for each site at a Tau/POPS ratio of 1:125 and [Tau] = 50 μ M.

3.1. Tau Engages in Site-Specific Direct Interaction at the Surface of Anionic Lipid Membranes

We first investigated the interaction of Tau with anionic LUVs made of pure POPS. We applied continuous wave-electron paramagnetic resonance (CW-EPR) spectroscopy to identify the direct interaction between Tau and lipid membranes at specific labeled sites.²⁷ We generated three Tau mutants amenable to single spin labeling at positions 322 (C291S mutation), 291 (C322S mutation), and 46 (S46C, C291S, and C322S mutations), referred to as Tau C322, Tau C291, and Tau C46, respectively. These sites span distinct regions of the protein: the R3 repeat, the R2 repeat, and the N-terminal region. For each mutant, we recorded and fitted the CW-EPR spectra in the absence and presence of POPS LUVs (Figure 1B,C). We observed a significant modification of the spin-label dynamics, quantified by its correlation time, at positions 291 and 322 (Figure 1E). This reflects a direct interaction between lipids and Tau in the repeat region but not at site 46. Note that the EPR line shape indicates that while C322 is stably bound to the

membrane, the site 291 is in exchange between a bound state (78.4 \pm 4.5% of the population) and free state (21.5 \pm 4.5% of the population) (Figure S3).

To further characterize Tau–lipid interactions, we measured the hyperfine coupling constant A_z , which reflects the polarity of the spin label's environment²⁸ and can be used to estimate membrane insertion of each labeled site. Both C291 and C322 showed a decrease in A_z upon lipid binding (from 36.9 to 35.5 G for C291, and from 36.9 to 35.4 G for C322) (Figure 1F), i.e., a decrease in water accessibility. This A_z value suggests a significant embedding in the membrane moiety.^{29,30} Conversely, C46, which does not directly interact with POPS (Figure 1C), exhibited a slight increase in A_z (Figures 1F and S4), reflecting a small increase in water exposure. This observation likely reflects an indirect effect of POPS binding, whereby membrane interaction of the R2 and R3 regions induces a global conformational rearrangement that increases solvent exposure of the N-terminal region.

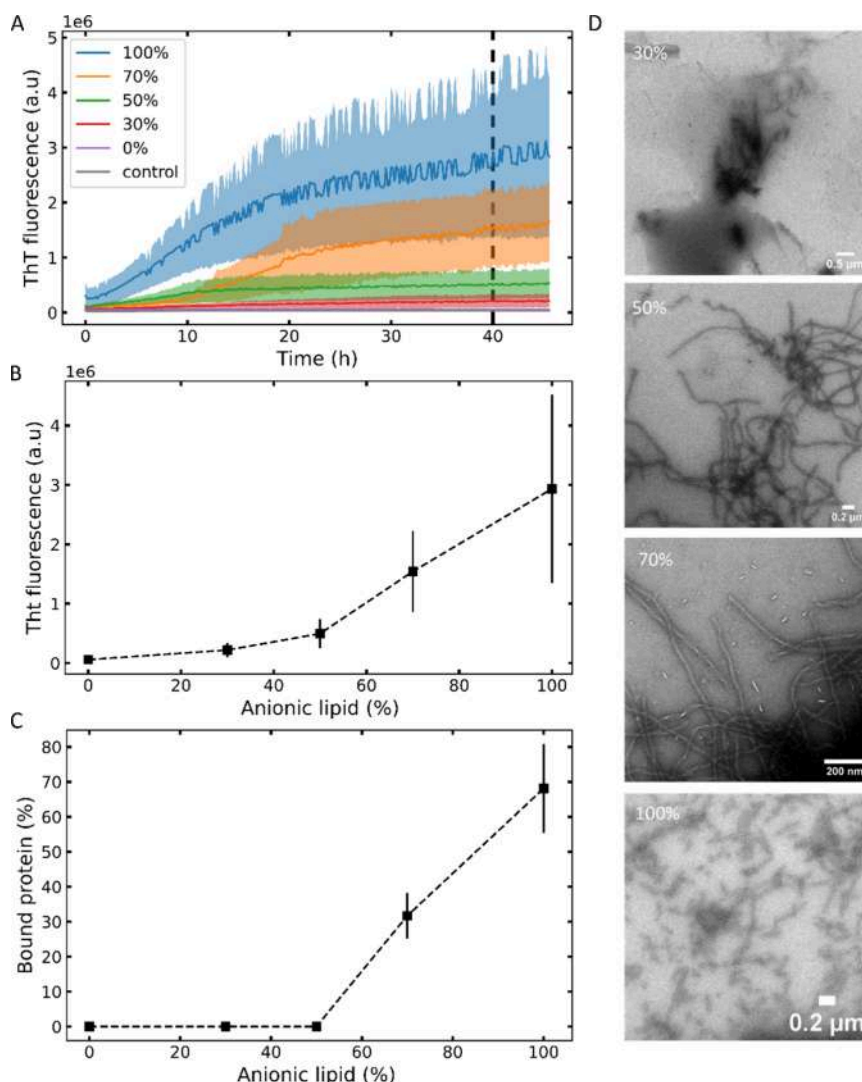


Figure 2. (A) ThT fluorescence over time measured in solutions of Tau P301L (20 μM) alone (gray) and incubated with POPS/POPC vesicles (0–100% POPS) (200 μM). Normalized ThT kinetics are represented in SI (Figure S5). (B) ThT fluorescence intensity after 40 h of incubation as a function of POPS percentage in LUVs. (C) Fraction of Tau P301L C322 bound to membranes, quantified by CW-EPR after 10 min of incubation as a function of POPS percentage in LUVs. (D) TEM image of Tau P301L incubated with POPS/POPC LUVs (30–100%) for 40h show the presence of fibrillar amyloid assemblies at 50% and above. In panels A–D, [Tau] = 20 μM, in panel C, [Tau] = 25 μM.

Those EPR observations point to the binding, and further insertion, of specific regions of Tau, at sites C291 and C322, in negatively charged membranes. To further probe this specificity, we performed similar experiments with fully zwitterionic POPC membranes. POPC LUVs did not lead to any significant change in spin dynamics for all probed sites of Tau (Figure 1D), suggesting that zwitterionic lipids cannot promote Tau-lipid interactions, and further confirming the key role of anionic lipids. In the next sections, we used Tau labeled at position 322 in order to gain insights into the relationship between Tau-lipid interaction and aggregation.

3.2. Anionic Lipids within the Membrane Are Required to Trigger Aggregation

To probe the influence of lipid vesicles with different anionic contents on Tau aggregation, we incubated Tau P301L with LUVs of various POPS/POPC molar ratios (from 0 to 100%), at a 1:10 protein/lipid ratio. We monitored Thioflavin T (ThT) fluorescence (Figure 2A,B) and imaged the samples after 40 h by TEM (Figure 2D). No increase in ThT fluorescence was

observed when Tau P301L was incubated with nonanionic LUVs made of pure POPC. When the anionic lipid POPS is incorporated in the LUVs, we observed a significant increase of ThT fluorescence from 50% of POPS. Above this threshold, the ThT intensity increases, together with the fibril quantity observed by TEM (Figure 2D), suggesting that a minimum fraction of anionic lipids is required to induce Tau aggregation.

In parallel, we quantified the amount of protein bound to the lipid membrane using CW-EPR, based on a previously established methodology.²⁷ The Tau–membrane interaction was quantified 10 min after the incubation of Tau with the LUVs (Figure 2C), before amyloid fibrils could be seen. We found that Tau significantly interacts with the membrane only when POPS is present above 50%. This demonstrates that a minimum quantity of anionic lipids on the membrane surface is necessary to enable the interaction, which triggers the aggregation on the time scale of 10s of hours. We confirmed the importance of electrostatic forces, suggested by the role of anionic lipids, by showing that both ThT fluorescence and binding decreased as salt concentration increased (Figure S6).

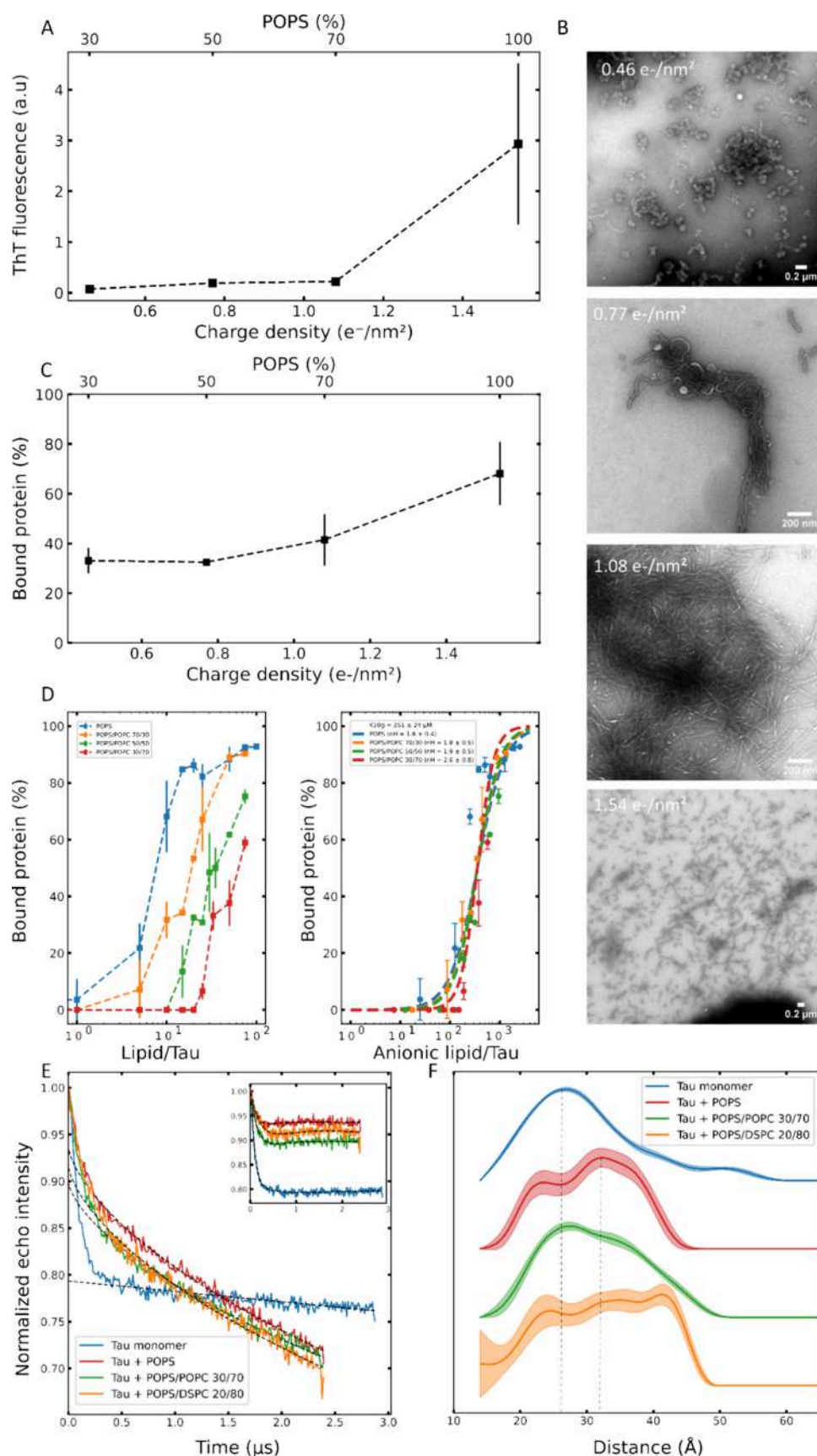


Figure 3. (A) ThT fluorescence intensity after 40 h of incubation, as a function of charge density (e^-/nm^2); $[\text{Tau}] = 20 \mu\text{M}$. ThT kinetics are represented in Figure S7. (B) TEM images of Tau P301L C322 incubated with POPS/POPC membranes at different charge densities. (C) Fraction of Tau P301L C322 bound to membranes, quantified by CW-EPR after 10 min of incubation as a function of charge density (e^-/nm^2). $[\text{Tau}] = 25 \mu\text{M}$. (D) Fraction of Tau P301L C322 as a function of the lipid/Tau ratio (left) and anionic lipid/Tau ratio (right). A Hill model is applied to fit data with a

Figure 3. continued

global K_{S0} and specific n_H for each data set. (E) Background-subtracted and normalized DEER time-domain signals. Experimental traces are shown in color; the corresponding background functions appear as dashed lines, and the fitted curves are displayed in the inset. (F) Distance distribution profiles of Tau P301L in solution (blue) and upon binding to LUVs of different compositions: POPS 100 (Lipid/Tau = 6; 35% bound, red), POPS/POPC 30/70 (Lipid/Tau = 33; 33% bound, green), and POPS/DSPC 20/80 (Lipid/Tau = 50; 30% bound, orange).

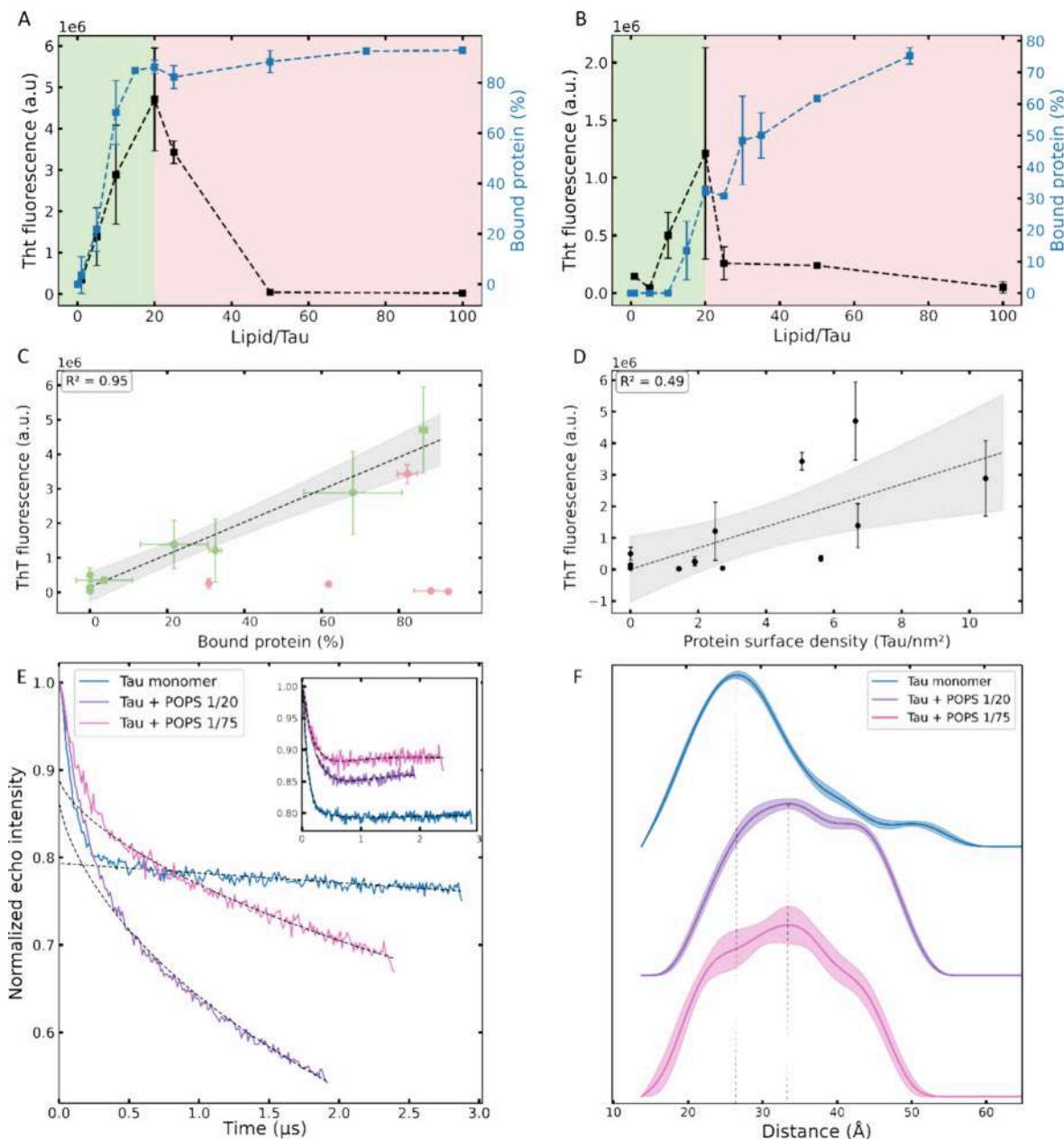


Figure 4. (A, B) ThT fluorescence intensity after 40 h of incubation, as a function of lipid/Tau ratios for POPS (A) and POPS/POPC 50/50 (B), with the corresponding fraction of bound protein determined by CW-EPR. (C) Correlation between ThT fluorescence at 40 h and the fraction of bound Tau with an overall fit yielding $r^2 = 0.95$. Green points correspond to low lipid/Tau ratios (green region in panels A and B), whereas red points represent high lipid/Tau ratios. (D) Correlation between ThT fluorescence at 40 h and the estimated surface density of membrane-bound Tau with an overall fit yielding $r^2 = 0.49$. Protein surface density was calculated by dividing the quantity of bound Tau by the quantity of lipid, assuming a headgroup area of 0.65 nm^2 per lipid. (E) Background-subtracted and normalized DEER time-domain signals. Experimental traces are shown in color, the corresponding background functions appear as dashed lines, and the fitted curves are displayed in the inset. (F) Distance distribution profiles of Tau P301L in solution (blue) and upon binding to LUVs of POPS with lipid/Tau = 20 ($86.2 \pm 2.6\%$ bound, $\alpha = 0.30$ purple) and lipid/Tau = 75 ($92.5 \pm 1.2\%$ bound, $\alpha = 0.15$, pink).

3.3. Minimum of Membrane Charge Density Is Required to Induce Tau Aggregation

After showing the critical role of anionic lipids in the membrane, we wanted to refine the mechanisms at play by looking at the effect of (i) the density of anionic lipids at the membrane surface and (ii) the quantity of lipids available per Tau protein.

We first designed experiments in which the number of POPS molecules per Tau monomer was held constant at 10, while the surface density of the POPS was modulated by dilution with neutral POPC lipids. Charge density values were calculated assuming a headgroup area of 0.65 nm² per POPS and one negative charge per molecule.³¹

As shown in Figure 3A, the ThT fluorescence at 40 h increases with charge density. This increase was significant at 1.5 e[−]/nm², corresponding to 100% of POPS, which is consistent with the presence of fibrils observed by TEM (Figure 3B). There is a threshold charge density required to trigger Tau aggregation, highlighting that nucleation of amyloid formation depends on the proximity of the interacting charges at the membrane surface.

In parallel, we measured the amount of bound Tau 10 min after incubation by CW-EPR experiments (Figure 3C). It revealed that a significant population of Tau remains bound to the LUVs across all tested charge densities. We further characterized binding properties by performing a full lipid titration with membranes exhibiting different charge densities (Figure 3D). We observed that binding curves against anionic lipids (Figure 3D, right graph) are similar regardless of the anionic content, suggesting that Tau's capacity to bind LUVs is independent of charge density. Moreover, we could fit the binding curves with a Hill model, using a global K₅₀ for all membrane compositions (Figure 3D, right graph). We found a K₅₀ of 351 ± 24 μM and a Hill coefficient varying from 1.6 to 2.6. Taken together, these results show that binding is dictated by the amount of charge (i.e., affinity is independent of charge density), but whether or not this interaction leads to aggregation depends on the membrane charge density. To understand how membrane charge density modulates aggregation, we next characterized Tau conformation, as specific conformational signatures have previously been reported to correlate with aggregation propensity.³²

3.4. High Membrane Charge Density Triggers Aggregation by Favoring Nucleation-Competent Tau Conformations

We employed double electron–electron resonance (DEER) spectroscopy to measure intramolecular distance distributions, which can capture the conformational ensemble of IDPs. Briefly, DEER allows the measurement of the distance distribution between two spin labels tethered to a protein at relevant positions.³³ We focus on the distances around the PHF6 motif (V306–K311), a key amyloidogenic region, which have been shown to reflect on aggregation propensity.^{32,34} For this purpose, we introduced cysteine mutations at positions V300C and V313C (termed Tau-300C-313C), followed by spin labeling of these residues.

In order to understand the aggregation-triggering capacity of membranes harboring high surface density, we assessed the Tau conformation in interaction with different membrane compositions. Specifically, we measured DEER in conditions where Tau is bound to the same extent (35% bound protein) to membranes containing either 100% POPS (high charge density, triggering aggregation) and 30% POPS (low charge density, incapable of triggering aggregation) (Figure 3E).

For Tau monomers, the distribution is centered around 28 Å (blue curve, Figure 3F), consistent with a compact conformation observed previously.³⁵ When LUVs composed of 100% POPS are used, a clear shift is observed toward longer distances, with a dominant population around 32 Å (red curve), while no change in the secondary structure is observed by CD (Figure S8). In contrast, with LUVs at 30% POPS, the population at 28 Å remains predominant (green curve), indicating that the majority of the Tau molecules retain a compact, monomer-like conformation. The observation that a distance increase occurs only in the presence of 100% POPS membrane shows that it is the high charge density that enables a conformational rearrangement toward extended, aggregation-prone, populations.

3.5. Interplay of Binding and Surface Organization Defines the Tau Aggregation Window

Next, we investigated how the amount of lipids available per Tau molecule influences amyloid formation. We titrated Tau with increasing amount of lipid vesicles, made of 100% POPS (Figure 4A) or 50/50 POPS/POPC (Figure 4B). We measured both the proteins binding to membrane 10 min after incubation and the ThT fluorescence at 40 h as a function of lipid/Tau. The reported ThT intensity exhibits a “bell shape” where the fluorescence increases with the lipid/Tau ratio at a low ratio, before decreasing at a high lipid/Tau ratio (Figure 4A,B). We rationalized this behavior using the bound populations.

In a first regime, at a low lipid/Tau ratio (green zone in Figure 4A,B), ThT fluorescence increases with the binding, pointing toward a binding-limited behavior. In other words, for both membrane compositions, the quantity of lipids available for binding directly limits the quantity of fibers found in the final state. This is further shown by the good correlation found between binding and ThT in this regime (Figure 4C).

In a second phase (red zone in Figure 4A,B), while the bound population keeps increasing with an increasing amount of lipids, the fluorescent signal drops. This behavior cannot be explained by the lack of monomers in solution at high lipid/protein ratios, as proposed earlier,³⁶ as shown by the quantitative measurements of bound population. Indeed, for the POPS/POPC membrane (Figure 4B), we show that the optimal aggregation point occurs when about 60% of the protein is free in solution. Furthermore, for the POPS membrane (Figure 4A), roughly the same population of the bound protein is measured when aggregation is optimal (ratio 1:20) and when it is inhibited (ratio 1:50). Rather, we hypothesize that aggregation is inhibited at a high lipid/Tau ratio because Tau molecules are too far apart to nucleate aggregation. Indeed, as the lipid/Tau ratio increases, each protein has a larger lipid surface area available and the bound proteins are split apart.

To test this hypothesis of a space-limited regime, we calculated the lipid surface available per protein bound to the membrane surface (i.e., [bound protein]/[lipid]) for every condition, and we examined how it correlates with ThT intensity (Figure 4D). We found a positive correlation ($R^2 = 0.5$), suggesting that indeed the protein crowding at the membrane surface is critical. To further confirm this result, we used DEER to directly measure the protein local concentration at the membrane surface. The DEER signal contains information on both intramolecular interactions, used to assess protein conformation, and intermolecular interaction, reflecting intermonomer proximity.²⁵ The latter information is contained in the α parameter of the background (see the Methods). We measured DEER of Tau-300C-313C incubated with the POPS

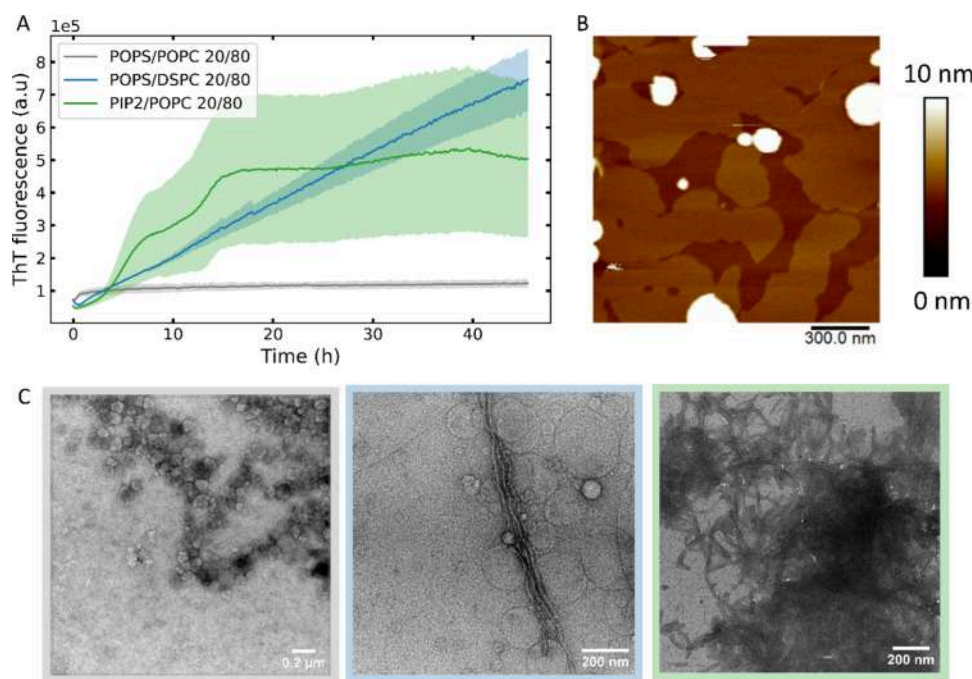


Figure 5. (A) ThT fluorescence over time measured for Tau P301L (20 μ M) in the presence of POPS/POPC (20/80, gray), PIP2/POPC (20/80, green), and POPS/DSPC (20/80, blue) LUVs at a lipid/Tau ratio of 10. (B) AFM image of POPS/DSPC (50/50) LUVs, showing evidence of phase separation. (C) TEM images of Tau P301L incubated for 40 h with PIP2/POPC (green), POPS/POPC (gray), and POPS/DSPC (phase separation, blue) vesicles. Fibrillar assemblies are observed under conditions associated with high local anionic charge density.

membrane at a Tau/lipid ratio of 1:20 (aggregation, $86 \pm 2.6\%$ bound) and 1:75 (no aggregation, $92.5 \pm 1.2\%$ bound) (Figure 4E,F). As expected from a high-charge-density membrane, in both conditions, Tau exhibits an open conformation (Figure 4F). When extracting the α parameter from the background (Figure 4E), we found α values of 0.15 for 1:75 and 0.30 for 1:20, demonstrating that the effective local concentration of Tau is significantly higher at a Tau/lipid ratio 1:20 compared to 1:75. This result further reinforces the hypothesis that the local density of the membrane-bound protein is critical to nucleate aggregation.

Based on these results, we can establish a general mechanism of membrane-induced Tau aggregation. First, Tau is recruited to the membrane mostly by electrostatic interactions with anionic lipids. This interaction populates Tau-aggregation-prone conformers only when the charge density at the membrane surface is high (50% POPS or higher). Then, the “activated” bound Tau molecules can efficiently nucleate aggregation once they are in the proximity of one another at the membrane surface. In the next section, we explored how this high-charge-density condition could be fulfilled in more physiological cellular conditions.

3.6. Local High Charge Density at the Membrane Surface Enables Amyloid Nucleation

In neuronal membranes, there are mostly two anionic lipids, POPS and PIP2. PIP2 differs from POPS because it contains three negative charges on its head, while POPS has only one. We demonstrated that the presence of PIP2 in a POPC LUVs at concentration as low as 20% has the capacity to induce Tau P301L aggregation, as shown in Figure 5A,C. This contrasts with the previous finding that at least 50% of POPS was necessary to reach the critical charge density necessary to trigger amyloid formation (Figure 2B). Thus, the presence of three anionic

charges on PIP2 plays the role of a cluster of charges at the membrane that facilitate Tau aggregation.

To highlight the relevance of charge density in a cellular context, we investigated the naturally occurring phenomenon of lipid phase separation that can lead to local concentration of particular lipids and their associated proteins.³⁷ We studied LUVs with DSPC, a zwitterionic lipid with a gel-to-fluid phase transition temperature of 55 °C. Unlike POPC, DSPC remains in a gel phase at both room temperature and 37 °C. To confirm the presence of charge patches in POPS/DSPC membranes, we performed AFM on supported lipid bilayers formed by depositing POPS/DSPC and POPS/POPC SUVs onto mica. AFM imaging revealed phase separation in POPS/DSPC bilayers (Figures 5B and S9), whereas POPS/POPC showed a homogeneous distribution (Figure S9). When Tau P301L was incubated with POPS/DSPC (20/80), we observed aggregation, as demonstrated by ThT kinetics (Figure 5A) and the presence of fibrils, as observed by TEM (Figure 5C). This contrasts with the incubation of Tau with the same amount of POPS in a homogeneous phase that did not trigger aggregation (gray curve, Figure 5A). Consistent with this behavior, we found that LUVs composed of POPS/DSPC (20/80) were capable of inducing Tau conformation rearrangement (Figure 3F, orange curve), which was otherwise not possible in homogeneous membranes. These results show that LUVs with low proportions of POPS, which are more physiological for neuronal membranes, are able to induce Tau aggregation given that the anionic lipids are locally concentrated. Overall, we show that Tau aggregation can be triggered even at low overall anionic lipid levels, provided that local charge density is sufficiently high.

4. DISCUSSION

In this study, we investigated the interaction and aggregation behavior of the longest isoform of Tau in the presence of lipid

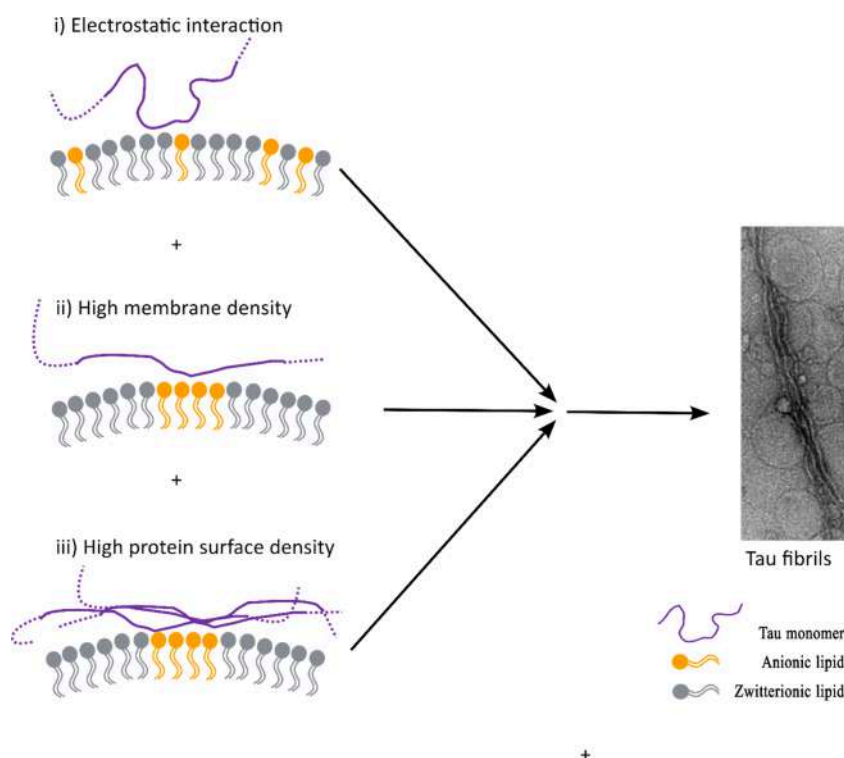


Figure 6. Proposed mechanism model of membrane-induced Tau aggregation. Efficient membrane-induced Tau aggregation requires: (i) recruitment of the protein at the membrane via anionic lipids, (ii) high charge density at the membrane surface to enable Tau conformation rearrangement, and (iii) protein crowding at the membrane surface.

membranes of varying compositions. Using a combination of biophysical techniques, we examined how Tau responds to changes in the membrane charge content, lipid/Tau ratios, and charge density. This systematic approach allowed us to dissect the role of lipid composition in modulating Tau aggregation.

Tau aggregation on lipid vesicles can be described as a stepwise process integrating both binding and spatial organization (Figure 6). Tau interacts with lipid membranes via electrostatic interaction with anionic lipids, as demonstrated by the absence of interaction with zwitterionic membranes (Figure 1) and the loss of interaction upon salt addition (Figure S6). This interaction is fairly independent of the anionic lipid organization at the surface, as seen by similar binding curves for different membrane compositions (Figure 3D). This interaction leads to aggregation only when two conditions are fulfilled (Figure 6). First, the charge density at the membrane surface needs to be high (Figure 3A) in order to induce a conformational rearrangement of Tau toward an open, aggregation-prone conformation (Figure 3F). Second, the Tau molecules, in their aggregation-prone conformation, need to be in close proximity to the membrane surface in order to nucleate aggregation (Figure 4).

A bell-shaped behavior, where aggregation peaks at an optimal inducer-to-protein ratio before declining, is a common signature across different inducers, including Heparin^{34,38,39} and acid arachidonic acid.³⁹ Here, by quantifying the amount of membrane-bound Tau proteins, we could directly explain this behavior (Figure 4). At a low lipid/Tau ratio, which we referred to as the binding-limited regime, Tau is scarcely bound to the membrane, leading to inefficient aggregate formation. At a high membrane/Tau ratio, referred to as the crowding-limited regime, the abundance of the membrane increases the membrane surface available per Tau molecule. This reduces

the proximity between Tau molecules, which appears to be necessary to nucleate aggregation. The optimal aggregation condition is reached when Tau molecules are sufficiently bound and are closely packed on the membranes. We argue that the same regimes could explain the behavior for other cofactors. In particular, the crowding-limited regime corresponds for heparin to conditions where single Tau proteins are interacting with an heparin molecule, leading to the formation of off-pathway complexes.³⁸ α -synuclein incubated with DMPS membranes showed the same bell-shaped behavior.³⁶ The decrease in aggregation in excess of membranes was interpreted as a lack of monomers in solution. Here, by quantifying the amount of free monomers, we unambiguously highlighted a distinct mechanism, since the quantity of free monomers was similar between optimal aggregation condition and the higher membrane/Tau ratio (Figure 4A). Furthermore, a similar bell-shaped dependence has been observed for the Tau–DMPS interaction, where membrane-induced fibrillation is strictly governed by the P:L ratio: high ratios promote assembly via macromolecular crowding, while low ratios prevent aggregation by maintaining protein separation.⁴⁰

Tau aggregation kinetics were analyzed by plotting the normalized ThT traces in different lipid concentrations (Figure S5). Although the ThT fluorescence shows different plateau levels (reported in Figures 2–4), the kinetics is essentially unaffected by lipid composition across the different POPS proportions. This indicates that, in our conditions, the observed modulation of Tau aggregation by the membrane is not a kinetic but rather thermodynamic process. The membrane composition does not significantly modulate the nucleation rates but the population of the final product. The finding that, in the binding-limited regime, the quantity of fibrils formed is directly related to the quantity of anionic lipids available (Figure 4A), suggests that

the anionic lipids are limiting reactants that are consumed, i.e., they are no longer available once aggregation proceeds. In other words, in these conditions, the membranes are not a catalytic factor as they become inactive after inducing Tau aggregation. This is consistent with the previous finding that Tau can strip anionic lipids from the supported bilayer.⁴¹ It also suggests a similar mechanism than what was observed for heparin and RNA cofactors.⁴²

Tau–anionic membrane interactions have been shown to promote structural changes in Tau, including compaction,⁴³ α -helix formation,^{44–46} and β -structure transitions.⁴⁶ Here, we showed that the lipid bilayer may induce specific conformational rearrangements around the PHF6 motif. In solution, Tau adopts a compact conformation (~ 28 Å), consistent with an aggregation-incompetent state characterized in previous studies with Tau fragments.³² Upon binding to membranes with high local anionic charge density, we observed a shift toward extended distances (~ 35 – 40 Å), indicative of an opening around the PHF6 region. This transition is expected to facilitate the accessibility of the hydrophobic hexapeptide, thus facilitating intermolecular interactions and nucleation.⁴⁷ In parallel, we performed circular dichroism (CD) experiments to monitor the secondary structure formation of Tau upon lipid binding. We showed that Tau remains predominantly in a random-coil conformation at the same incubation time point at which DEER reveals an extended conformation (Figure S8). The opening of Tau detected by DEER therefore represents an early conformational rearrangement that precedes β -sheet formation during amyloid fibril assembly. Similar conformational transitions have been reported in the presence of heparin, which also triggers Tau aggregation.^{32,48} Disease-associated mutations were also shown to trigger local and global extension,^{47,49} pointing to a general signature of aggregation-promoting conditions. The extended conformation is measured here prior to detectable fibril formation and is likely to be part of the nucleation-competent ensemble. Our findings suggest that lipid membranes act as environmental triggers capable of modulating the Tau conformational landscape, with the lipid local organization as a key modulator (Figure 3F).

The work presented here was performed on Tau containing the mutation P301L, known to favor protein aggregation,³ because it provided reliable and tunable aggregation with membranes. Membrane vesicles can also induce aggregation of WT Tau,⁴⁰ and we expect that the model of charge-driven binding followed by intra- and intermolecular rearrangement will be valid for WT. However, it will be interesting to test precisely on which steps the different disease-associated mutations act to modulate membrane-induced aggregation.

We showed that the local concentration of Tau at the membrane surface is critical (Figure 4D,F), likely because it promotes productive intermolecular interactions, ultimately enabling the formation of nucleation-competent clusters. In this context, anionic membranes act as key mediators of Tau–Tau interactions by providing active surfaces that facilitate protein–protein condensation and association, further reinforcing previous studies on Tau fragments.¹⁸

Using our model, we predicted and tested that membrane heterogeneity, which changes local surface charge, plays a central role in modulating Tau–lipid assemblies. In cellular membranes, such heterogeneity often arises in the form of lipid rafts, which are dynamic microdomains that can be enriched in cholesterol, sphingolipids, and specific membrane proteins.^{50,51} While rafts are defined by cholesterol and sphingolipid enrichment, they can

also selectively sequester other lipids, including anionic species like phosphatidylserine (PS) and phosphoinositides (PIPs), thereby creating localized “charge patches” with high surface charge density.^{52,53} It has been shown in vitro that cholesterol-containing high-curvature membranes induce Tau amyloid fibrils, at a low proportion of PS.⁵⁴ Cholesterol may act by promoting the formation of lipid domains that locally increase PS density.⁵⁵ This phenomenon is particularly relevant in the context of neurodegenerative diseases, where dysregulation of lipid metabolism is a well-established pathological feature.¹⁰ Thus, the ability of membranes to form localized charge patches provides a plausible mechanism by which lipid metabolism and raft dynamics can directly influence Tau aggregation. Further systematic investigations will be essential to confirm the effect of membrane composition and organization directly in cellular environments.

■ ASSOCIATED CONTENT

Supporting Information

The Supporting Information is available free of charge at <https://pubs.acs.org/doi/10.1021/jacsau.6c00374>.

Supplementary figures supporting data treatment and interpretation (PDF)

■ AUTHOR INFORMATION

Corresponding Author

Yann Fichou – CNRS, Bordeaux INP, CBMN, UMR 5248, IECB, University of Bordeaux, Pessac F-33600, France; orcid.org/0000-0002-6520-0041; Email: y.fichou@iecb.u-bordeaux.fr

Authors

Clara Pierrsson – CNRS, Bordeaux INP, CBMN, UMR 5248, IECB, University of Bordeaux, Pessac F-33600, France

Victoria Lublin – CNRS, Bordeaux INP, CBMN, UMR 5248, IECB, University of Bordeaux, Pessac F-33600, France

Mathieu Duttine – CNRS, Bordeaux INP, ICMCB, UMR 5026, University of Bordeaux, Pessac F-33600, France;

orcid.org/0000-0002-6120-8716

Lucie Khentemourian – CNRS, Bordeaux INP, CBMN, UMR 5248, University of Bordeaux, Pessac F-33600, France

Antoine Loquet – CNRS, Bordeaux INP, CBMN, UMR 5248, IECB, University of Bordeaux, Pessac F-33600, France;

orcid.org/0000-0001-7176-7813

Marion Mathelié-Guinlet – CNRS, Bordeaux INP, CBMN, UMR 5248, University of Bordeaux, Pessac F-33600, France

Complete contact information is available at:

<https://pubs.acs.org/doi/10.1021/jacsau.6c00374>

Author Contributions

CRediT: Victoria Lublin data curation.

Notes

The authors declare no competing financial interest.

■ ACKNOWLEDGMENTS

Y.F. thanks the European Research Council (Grant 101040138), the Fondation Vaincre Alzheimer, and the Federation of European Biochemical Societies for their financial support. The authors acknowledge Guillaume Gerbaud and the IR INFRANALYTICS FR2054 for financial support to conduct

DEER experiments. We are grateful to Isabel Alves and Eric Dufourc from CBMN for insightful discussions on lipid behavior in membranes. We would like to thank Dr. Rodophe Cl  rac and Mr. Mathieu Rouzi  res from the Centre de Recherche Paul Pascal (UMR5031) for privileged access to the EPR spectrometer.

REFERENCES

- (1) Wang, Y.; Mandelkow, E. Tau in Physiology and Pathology. *Nat. Rev. Neurosci.* **2016**, *17* (1), 22–35.
- (2) Fitzpatrick, A. W. P.; Debelouchina, G. T.; Bayro, M. J.; Clare, D. K.; Caporini, M. A.; Bajaj, V. S.; Jaroniec, C. P.; Wang, L.; Ladizhansky, V.; M  ller, S. A.; MacPhee, C. E.; Waudby, C. A.; Mott, H. R.; De Simone, A.; Knowles, T. P. J.; Saibil, H. R.; Vendruscolo, M.; Orlova, E. V.; Griffin, R. G.; Dobson, C. M. Atomic Structure and Hierarchical Assembly of a Cross- β Amyloid Fibril. *Proc. Natl. Acad. Sci. U.S.A.* **2013**, *110* (14), 5468–5473.
- (3) Nacharaju, P.; Lewis, J.; Easson, C.; Yen, S.; Hackett, J.; Hutton, M.; Yen, S.-H. Accelerated Filament Formation from Tau Protein with Specific FTDP-17 Missense Mutations. *FEBS Lett.* **1999**, *447* (2–3), 195–199.
- (4) Falcon, B.; Zhang, W.; Murzin, A. G.; Murshudov, G.; Garringer, H. J.; Vidal, R.; Crowther, R. A.; Ghetti, B.; Scheres, S. H. W.; Goedert, M. Structures of Filaments from Pick’s Disease Reveal a Novel Tau Protein Fold. *Nature* **2018**, *561* (7721), 137.
- (5) Falcon, B.; Zivanov, J.; Zhang, W.; Murzin, A. G.; Garringer, H. J.; Vidal, R.; Crowther, R. A.; Newell, K. L.; Ghetti, B.; Goedert, M.; Scheres, S. H. W. Novel Tau Filament Fold in Chronic Traumatic Encephalopathy Encloses Hydrophobic Molecules. *Nature* **2019**, *568* (7752), 420.
- (6) Fitzpatrick, A. W. P.; Falcon, B.; He, S.; Murzin, A. G.; Murshudov, G.; Garringer, H. J.; Crowther, R. A.; Ghetti, B.; Goedert, M.; Scheres, S. H. W. Cryo-EM Structures of Tau Filaments from Alzheimer’s Disease. *Nature* **2017**, *547* (7662), 185–190.
- (7) Shi, Y.; Zhang, W.; Yang, Y.; Murzin, A. G.; Falcon, B.; Kotecha, A.; van Beers, M.; Tarutani, A.; Kametani, F.; Garringer, H. J.; Vidal, R.; Hallinan, G. I.; Lashley, T.; Saito, Y.; Murayama, S.; Yoshida, M.; Tanaka, H.; Kakita, A.; Ikeuchi, T.; Robinson, A. C.; Mann, D. M. A.; Kovacs, G. G.; Revesz, T.; Ghetti, B.; Hasegawa, M.; Goedert, M.; Scheres, S. H. W. Structure-Based Classification of Tauopathies. *Nature* **2021**, *598* (7880), 359–363.
- (8) Zhang, W.; Tarutani, A.; Newell, K. L.; Murzin, A. G.; Matsubara, T.; Falcon, B.; Vidal, R.; Garringer, H. J.; Shi, Y.; Ikeuchi, T.; Murayama, S.; Ghetti, B.; Hasegawa, M.; Goedert, M.; Scheres, S. H. W. Novel Tau Filament Fold in Corticobasal Degeneration. *Nature* **2020**, *580* (7802), 283–287.
- (9) Gellermann, G. P.; Appel, T. R.; Davies, P.; Diekmann, S. Paired Helical Filaments Contain Small Amounts of Cholesterol, Phosphatidylcholine and Sphingolipids. *Biol. Chem.* **2006**, *387* (9), 1267.
- (10) Ole  sov  , D.; Dobe  sov  , D.; Majerov  , P.; Brumarov  , R.; Kvasni  ka, A.; Kouril,   .; Stevens, E.; Hanes, J.; Fialov  ,   .; Michaliov  , A.; Pie  tansk  , J.;   insk  , J.; Ka  novsk  , P.; Friedeck  , D.; Kov   , A. Changes in Lipid Metabolism Track with the Progression of Neurofibrillary Pathology in Tauopathies. *J. Neuroinflammation* **2024**, *21* (1), 78.
- (11) Fried, B.; Antonschmidt, L.; Dienemann, C.; Geraets, J. A.; Najbauer, E. E.; Matthes, D.; de Groot, B. L.; Andreas, L. B.; Becker, S.; Griesinger, C.; Schr  der, G. F. The 3D Structure of Lipidic Fibrils of α -Synuclein. *Nat. Commun.* **2022**, *13* (1), 6810.
- (12) Brandt, R.; L  ger, J.; Lee, G. Interaction of Tau with the Neural Plasma Membrane Mediated by Tau’s Amino-Terminal Projection Domain. *J. Cell Biol.* **1995**, *131* (5), 1327–1340.
- (13) Chai, X.; Dage, J. L.; Citron, M. Constitutive Secretion of Tau Protein by an Unconventional Mechanism. *Neurobiology of Disease* **2012**, *48* (3), 356–366.
- (14) Katsinelos, T.; Zeitler, M.; Dimou, E.; Karakatsani, A.; M  ller, H.-M.; Nachman, E.; Steringer, J. P.; Ruiz de Almodovar, C.; Nickel, W.; Jahn, T. R. Unconventional Secretion Mediates the Trans-Cellular Spreading of Tau. *Cell Reports* **2018**, *23* (7), 2039–2055.
- (15) Wang, Y.; Balaji, V.; Kaniyappan, S.; Kr  ger, L.; Irsen, S.; Tepper, K.; Chandupatla, R.; Maetzler, W.; Schneider, A.; Mandelkow, E.; Mandelkow, E.-M. The Release and Trans-Synaptic Transmission of Tau via Exosomes. *Mol. Neurodegeneration* **2017**, *12* (1), 5.
- (16) Kawarabayashi, T.; Shoji, M.; Younkin, L. H.; Wen-Lang, L.; Dickson, D. W.; Murakami, T.; Matsubara, E.; Abe, K.; Ashe, K. H.; Younkin, S. G. Dimeric Amyloid Beta Protein Rapidly Accumulates in Lipid Rafts Followed by Apolipoprotein E and Phosphorylated Tau Accumulation in the Tg2576 Mouse Model of Alzheimer’s Disease. *J. Neurosci.* **2004**, *24* (15), 3801–3809.
- (17) Dicke, S. S.; Tatge, L.; Engen, P. E.; Culp, M.; Masterson, L. R. Isothermal Titration Calorimetry and Vesicle Leakage Assays Highlight the Differential Behaviors of Tau Repeat Segments upon Interaction with Anionic Lipid Membranes. *Biochem. Biophys. Res. Commun.* **2017**, *493* (4), 1504–1509.
- (18) Elbaum-Garfinkle, S.; Ramlall, T.; Rhoades, E. The Role of the Lipid Bilayer in Tau Aggregation. *Biophys. J.* **2010**, *98* (11), 2722–2730.
- (19) Talaga, D.; Smeralda, W.; Lescos, L.; Hunel, J.; Lepejova-Caudy, N.; Cullin, C.; Bonhommeau, S.; Lecomte, S. PIP2 Phospholipid-Induced Aggregation of Tau Filaments Probed by Tip-Enhanced Raman Spectroscopy. *Angew. Chem.* **2018**, *130* (48), 15964–15968.
- (20) Ali, A.; Holman, A. P.; Rodriguez, A.; Matveyenko, M.; Kurouski, D. Tubulin-Binding Region Alters Tau–Lipid Interactions and Changes Toxicity of Tau Fibrils Formed in the Presence of Phosphatidylserine Lipids. *Protein Sci.* **2024**, *33* (7), No. e5078.
- (21) Rouser, G.; Fleischer, S.; Yamamoto, A. Two Dimensional Thin Layer Chromatographic Separation of Polar Lipids and Determination of Phospholipids by Phosphorus Analysis of Spots. *Lipids* **1970**, *5* (5), 494–496.
- (22) Xue, C.; Lin, T. Y.; Chang, D.; Guo, Z. Thioflavin T as an Amyloid Dye: Fibril Quantification, Optimal Concentration and Effect on Aggregation. *Royal Society Open Science* **2017**, *4* (1), No. 160696.
- (23) Etienne, E.; Pierro, A.; Tamburrini, K. C.; Bonucci, A.; Mileo, E.; Martinho, M.; Belle, V. Guidelines for the Simulations of Nitroxide X-Band CW EPR Spectra from Site-Directed Spin Labeling Experiments Using SimLabel. *Molecules* **2023**, *28* (3), 1348.
- (24) Milov, A. D.; Maryasov, A. G.; Tsvetkov, Y. D. Pulsed Electron Double Resonance (PELDOR) and Its Applications in Free-Radicals Research. *Appl. Magn. Reson.* **1998**, *15* (1), 107–143.
- (25) Tsay, K.; Keller, T.; Fichou, Y.; Freed, J. H.; Han, S.-I.; Srivastava, M. Localized Reconstruction of Multimodal Distance Distribution from DEER Data of Biopolymers. *bioRxiv* 2025. .
- (26) Barghorn, S.; Zheng-Fischh  fer, Q.; Ackmann, M.; Biernat, J.; von Bergen, M.; Mandelkow, E.-M.; Mandelkow, E. Structure, Microtubule Interactions, and Paired Helical Filament Aggregation by Tau Mutants of Frontotemporal Dementias. *Biochemistry* **2000**, *39* (38), 11714–11721.
- (27) Pierrson, C.; Prakash, S.; Lublin, V.; Rossotti, M.; Fischer, B.; Srivastava, M.; Fichou, Y. Development of an EPR-Based Methodology to Study Protein-Lipid Interaction. *bioRxiv* 2025. .
- (28) Subczynski, W. K.; Wisniewska, A.; Yin, J.-J.; Hyde, J. S.; Kusumi, A. Hydrophobic Barriers of Lipid Bilayer Membranes Formed by Reduction of Water Penetration by Alkyl Chain Unsaturation and Cholesterol. *Biochemistry* **1994**, *33* (24), 7670–7681.
- (29) Steinhoff, H.-J.; Savitsky, A.; Wegener, C.; Pfeiffer, M.; Plato, M.; M  bius, K. High-Field EPR Studies of the Structure and Conformational Changes of Site-Directed Spin Labeled Bacteriorhodopsin. *Biochimica et Biophysica Acta (BBA) - Bioenergetics* **2000**, *1457* (3), 253–262.
- (30) Volkov, A.; Dockter, C.; Bund, T.; Paulsen, H.; Jeschke, G. Pulsed EPR Determination of Water Accessibility to Spin-Labeled Amino Acid Residues in LHCIIB. *Biophys. J.* **2009**, *96* (3), 1124–1141.
- (31) Chowdhury, U. D.; Paul, A.; Bhargava, B. L. The Effect of Lipid Composition on the Dynamics of Tau Fibrils. *Proteins: Struct., Funct., Bioinf.* **2022**, *90* (12), 2103–2115.
- (32) Eschmann, N. A.; Georgieva, E. R.; Ganguly, P.; Borbat, P. P.; Rappaport, M. D.; Akdogan, Y.; Freed, J. H.; Shea, J.-E.; Han, S.

- 860 Signature of an Aggregation-Prone Conformation of Tau. *Sci. Rep.* **2017**,
861 7 (1), 44739.
- 862 (33) Jeschke, G. DEER Distance Measurements on Proteins. *Annu.*
863 *Rev. Phys. Chem.* **2012**, 63, 419–446.
- 864 (34) Fichou, Y.; Oberholtzer, Z. R.; Ngo, H.; Cheng, C.-Y.; Keller, T.
865 J.; Eschmann, N. A.; Han, S. Tau-Cofactor Complexes as Building
866 Blocks of Tau Fibrils. *Front. Neurosci.* **2019**, 13, 1339.
- 867 (35) Lin, Y.; Fichou, Y.; Zeng, Z.; Hu, N. Y.; Han, S. Electrostatically
868 Driven Complex Coacervation and Amyloid Aggregation of Tau Are
869 Independent Processes with Overlapping Conditions. *ACS Chem.*
870 *Neurosci.* **2020**, 11 (4), 615–627.
- 871 (36) Galvagnion, C.; Buell, A. K.; Meisl, G.; Michaels, T. C. T.;
872 Vendruscolo, M.; Knowles, T. P. J.; Dobson, C. M. Lipid Vesicles
873 Trigger α -Synuclein Aggregation by Stimulating Primary Nucleation.
874 *Nat. Chem. Biol.* **2015**, 11 (3), 229–234.
- 875 (37) Harayama, T.; Riezman, H. Understanding the Diversity of
876 Membrane Lipid Composition. *Nat. Rev. Mol. Cell Biol.* **2018**, 19 (5),
877 281–296.
- 878 (38) Ramachandran, G.; Udgaonkar, J. B. Understanding the Kinetic
879 Roles of the Inducer Heparin and of Rod-like Protofibrils during
880 Amyloid Fibril Formation by Tau Protein. *J. Biol. Chem.* **2011**, 286
881 (45), 38948–38959.
- 882 (39) Carlson, S. W.; Branden, M.; Voss, K.; Sun, Q.; Rankin, C. A.;
883 Gamblin, T. C. A Complex Mechanism for Inducer Mediated Tau
884 Polymerization†. *Biochemistry* **2007**, 46 (30), 8838–8849.
- 885 (40) Yao, Q.-Q.; Wen, J.; Perrett, S.; Wu, S. Distinct Lipid Membrane-
886 Mediated Pathways of Tau Assembly Revealed by Single-Molecule
887 Analysis. *Nanoscale* **2022**, 14 (12), 4604–4613.
- 888 (41) Ury-Thiery, V.; Fichou, Y.; Alves, I.; Molinari, M.; Lecomte, S.;
889 Feuille, C. Interaction of Full-Length Tau with Negatively Charged
890 Lipid Membranes Leads to Polymorphic Aggregates. *Nanoscale* **2024**,
891 16 (36), 17141–17153.
- 892 (42) Fichou, Y.; Lin, Y.; Rauch, J. N.; Vigers, M.; Zeng, Z.; Srivastava,
893 M.; Keller, T. J.; Freed, J. H.; Kosik, K. S.; Han, S. Cofactors Are
894 Essential Constituents of Stable and Seeding-Active Tau Fibrils. *Proc.*
895 *Natl. Acad. Sci. U.S.A.* **2018**, 115 (52), 13234–13239.
- 896 (43) Jones, E. M.; Dubey, M.; Camp, P. J.; Vernon, B. C.; Biernat, J.;
897 Mandelkow, E.; Majewski, J.; Chi, E. Y. Interaction of Tau Protein with
898 Model Lipid Membranes Induces Tau Structural Compaction and
899 Membrane Disruption. *Biochemistry* **2012**, 51 (12), 2539–2550.
- 900 (44) Barré, P.; Eliezer, D. Folding of the Repeat Domain of Tau Upon
901 Binding to Lipid Surfaces. *J. Mol. Biol.* **2006**, 362 (2), 312–326.
- 902 (45) Georgieva, E. R.; Xiao, S.; Borbat, P. P.; Freed, J. H.; Eliezer, D.
903 Tau Binds to Lipid Membrane Surfaces via Short Amphipathic Helices
904 Located in Its Microtubule-Binding Repeats. *Biophys. J.* **2014**, 107 (6),
905 1441–1452.
- 906 (46) Künze, G.; Barré, P.; Scheidt, H. A.; Thomas, L.; Eliezer, D.;
907 Huster, D. Binding of the Three-Repeat Domain of Tau to
908 Phospholipid Membranes Induces an Aggregated-like State of the
909 Protein. *Biochimica et Biophysica Acta (BBA) - Biomembranes* **2012**,
910 1818 (9), 2302–2313.
- 911 (47) Chen, D.; Drombosky, K. W.; Hou, Z.; Sari, L.; Kashmer, O. M.;
912 Ryder, B. D.; Perez, V. A.; Woodard, D. R.; Lin, M. M.; Diamond, M. I.;
913 Joachimiak, L. A. Tau Local Structure Shields an Amyloid-Forming
914 Motif and Controls Aggregation Propensity. *Nat. Commun.* **2019**, 10
915 (1), 2493.
- 916 (48) Elbaum-Garfinkle, S.; Rhoades, E. Identification of an
917 Aggregation-Prone Structure of Tau. *J. Am. Chem. Soc.* **2012**, 134
918 (40), 16607–16613.
- 919 (49) Pounot, K.; Piersson, C.; Goring, A. K.; Rosu, F.; Gabelica, V.;
920 Weik, M.; Han, S.; Fichou, Y. Mutations in Tau Protein Promote
921 Aggregation by Favoring Extended Conformations. *JACS Au* **2024**, 4
922 (1), 92–100.
- 923 (50) Rajendran, L.; Simons, K. Lipid Rafts and Membrane Dynamics.
924 *Journal of Cell Science* **2005**, 118 (6), 1099–1102.
- 925 (51) Cheng, X.; Smith, J. C. Biological Membrane Organization and
926 Cellular Signaling. *Chem. Rev.* **2019**, 119 (9), 5849–5880.
- 927 (52) Ingólfsson, H. I.; Melo, M. N.; van Eerden, F. J.; Arnarez, C.;
928 Lopez, C. A.; Wassenaar, T. A.; Periole, X.; de Vries, A. H.; Tieleman, D.
P.; Marrink, S. J. Lipid Organization of the Plasma Membrane. *J. Am.* 929
Chem. Soc. **2014**, 136 (41), 14554–14559. 930
- (53) Sonnino, S.; Prinetti, A. Lipids and Membrane Lateral 931
Organization. *Front. Physiol.* **2010**, 1, 153. 932
- (54) El Mammeri, N.; Gampp, O.; Duan, P.; Hong, M. Membrane- 933
Induced Tau Amyloid Fibrils. *Commun. Biol.* **2023**, 6 (1), 1–12. 934
- (55) Doktorova, M.; Heberle, F. A.; Kingston, R. L.; Khelashvili, G.; 935
Cuendet, M. A.; Wen, Y.; Katsaras, J.; Feigenson, G. W.; Vogt, V. M.; 936
Dick, R. A. Cholesterol Promotes Protein Binding by Affecting 937
Membrane Electrostatics and Solvation Properties. *Biophys. J.* **2017**, 938
113 (9), 2004–2015. 939